

A novel derivative of picolinic acid induces endoplasmic reticulum stress-mediated apoptosis in human non-small cell lung cancer cells: synthesis, docking study, and anticancer activity

Ali H. Abbas¹, Ammar A. Razzak Mahmood², Lubna H. Tahtamouni^{3,4}, Zainab A. Al-Mazaydeh³, Majdoleen S. Rammaha³, Fatima Alsoubani⁵, Rheda I. Al-bayati⁶

1 Department of Pharmaceutical Chemistry, College of Pharmacy, University of Tikrit, Tikrit/Salah-Aldin, 34001, Iraq

2 Department of Pharmaceutical Chemistry, College of Pharmacy-University of Baghdad, Baghdad, Bab-Al-Mouadam-10001, Iraq

3 Department of Biology and Biotechnology, Faculty of Science, the Hashemite University, Zarqa, Jordan

4 Department of Biochemistry and Molecular Biology, College of Natural Sciences, Colorado State University, Fort Collins, Colorado, USA

5 Department of Chemistry, the Hashemite University, Zarqa 13133, Jordan

6 Department of Chemistry, College of Science, Al-Mustansirya University, Baghdad, 10001, Iraq

Corresponding author: Ali H. Abbas (alih.phchm@tu.edu.iq)

Received 25 June 2021 ♦ Accepted 17 August 2021 ♦ Published 8 September 2021

Citation: Abbas AH, Razzak Mahmood AA, Tahtamouni LH, Al-Mazaydeh ZA, Rammaha MS, Alsoubani F, Al-bayati RI (2021) A novel derivative of picolinic acid induces endoplasmic reticulum stress-mediated apoptosis in human non-small cell lung cancer cells: synthesis, docking study, and anticancer activity. *Pharmacia* 68(3): 679–692. <https://doi.org/10.3897/pharmacia.68.e70654>

Abstract

Thirteen new derivatives of picolinic acid (4–7) were designed and synthesized from the starting parent molecule, picolinic acid. The new compounds were characterized by ATR-FTIR, ¹HNMR, and CHNS analysis. A molecular docking study was performed to evaluate the binding affinity of the synthesized compounds toward EGFR kinase domain that indicated occupation of the critical site of EGFR kinase pocket and excellent positioning of the compounds in the pocket. The cytotoxic activity of the compounds against two human cancer cell lines (A549 and MCF-7), the non-tumorigenic MCF10A cell line, and white blood cells (WBC) was evaluated using the MTT assay. Compound 5 showed anticancer activity against A549 lung cancer cells (IC₅₀ = 99.93 μM) but not against MCF-7 breast cancer cells or normal cells. Compound 5 mediated cytotoxicity in A549 lung cancer cells by inducing apoptotic cell death, as suggested by fragmented nuclei after DAPI staining, and agarose gel electrophoresis. Moreover, compound 5 triggered the activation of caspases 3, 4 and 9. However, compound 5 treatment did not affect the release of cytochrome c from the mitochondria to the cytosol, as compared to the vehicle-treated control cells. Nevertheless, compound 5-treated cells reported greater release of smac/DIABLO to the cytosol. In the same context, both compound 5 and thapsigargin (specific inhibitor of sarco/endoplasmic reticulum Ca²⁺-ATPase (SERCA)) enhanced eIF2 phosphorylation, reflecting the activation of the atypical ER stress pathway and the potential applicability of compound 5 in lung cancer treatment.

Keywords

Picolinic acid, ER stress pathway, Docking, A549 lung cancer cells

Introduction

The Global Cancer Observatory 2020 clearly reported that there were 19.3 million new cancer cases and nearly 10 million cancer deaths in 2020. Malignant diseases are a major cause of mortality and morbidity in every region of the world irrespective of the human development index (Sung et al. 2021). Several research groups worldwide continue their work on elucidating the molecular mechanisms implicated in carcinogenesis and cancer progression that are of key importance to cancer prevention and targeted treatment strategies (Golemis et al. 2018).

Lung cancer is the leading cause of cancer-related deaths globally, with an overall five-year survival rate of 15% (Zhang et al. 2020). Non-small cell lung carcinoma (NSCLC) accounts for roughly 75–80% of all lung cancers. Patients with NSCLC eventually develop resistance to chemotherapy drugs that compromises their efficacy and significantly reduces the survival time to only 8 to 10 months. In addition, 30–60% of patients with early-stage disease who undergo curative surgery develop recurrence. Thus, there is a clear need for additional and more appropriate treatments for advanced or recurrent NSCLCs (Da Cunha Santos et al. 2011).

Endoplasmic reticulum (ER) is a major organelle with several cellular functions and is a vital site for the maintenance of homeostasis. When ER-related pathways of protein folding regulation, post-translational changes, cellular metabolism and/or calcium signaling are disturbed, the accumulation of ER-related proteins might ultimately lead to ER stress (ERS). Under overwhelming ERS, the cells initiate autophagy, followed by large-scale degradation and apoptosis (Yu et al. 2016). Hypoxia, nutrient deprivation, radiotherapy, and chemotherapy are among the factors known to induce ERS, which in turn activates the unfolded protein response (UPR). Extensive and acute ER stress directs the UPR towards activation of death-triggering pathways. Accumulation of mis/unfolded proteins leads to phosphorylation of eukaryotic initiation factor 2 subunit a (eIF-2 α), activation of caspase 4 (Fu et al. 2015), and the release of second mitochondria-derived activator of caspase/direct inhibitor of apoptosis-binding protein with low isoelectric point (smac/ DIABLO) from the mitochondria which inactivates the inhibitors of apoptosis proteins (IAPs) that contribute to the activation of caspases (Parrish and Freel 2013). The ER has recently been recognized as a highly potential target for anti-cancer agents. Cytotoxic compounds trying to target ER often exhibit selectivity for cancer cells over non-cancer cells. Furthermore, the induction of ER stress frequently results in the death of immunogenic cells, offering another factor that contributes to the clinical efficacy of drugs that target this organelle (King and Wilson 2020).

The epidermal growth factor receptor (EGFR)/Her1/ ErbB1 is a cell-surface receptor that belongs to the ErbB family of tyrosine kinases. EGFR has earned a great attention as a molecular target in cancer therapy, owing to its abnormal expression (upregulation) in many epithelial tumors, and its influence on growth and survival in malignant

states (Wang 2017). EGFR mutations are the second most popular oncogenic incident in NSCLC. In the same regard, it is estimated that half of the cases of triple-negative breast cancer (TNBC), and inflammatory breast cancer (IBC) over-express EGFR (Masuda et al. 2012). Classical activating mutations (exon 19 deletions and L858R point mutation) comprise the vast majority of EGFR mutations and are well defined as strong predictors of good clinical response to EGFR tyrosine kinase inhibitors (TKIs). However, low-frequency mutations, including point mutations, deletions, insertions, and duplication, occur within the 18–25 exons of the EGFR gene in the NSCLC and thus, are linked to poor TKI responses (Harrison et al. 2020). EGFR-dependent tumors that are initially sensitive to EGFR TKIs develop a threonine 790 mutation. Substitution of this residue in EGFR with bulky methionine, may cause resistance by steric interference with TKI binding, as is shown to be the case with the TKI inhibitors gefitinib and erlotinib (Wheeler et al. 2010). Therefore, innovative compounds and drug combinations that induce cancer cell killing with new mechanisms of action hold a great promise to delay or overcome chemoresistance caused by the clinically used EGFR TKIs (Westover et al. 2018).

Picolinic acid (PA) has already been identified as an activator of macrophage pro-inflammatory functions, which provided the first indications of the independent bioactive properties of picolinic acid even in the absence of a co-stimulatory agent (Bosco et al. 2000). In addition, PA derivatives exhibited considerable antitumor and anti-angiogenic effects (Zeidan et al. 2019; Al-Saif et al. 2020; Bai et al. 2020; Tung et al. 2020; Xiong et al. 2020; Zheng et al. 2020). The current research was performed to design and synthesize new picolinic acid derivatives, and to assess their antitumor activity, with additional verification using a docking study.

Materials and methods

Chemical synthesis

Picolinic acid was purchased from Sigma-Aldrich. Reactions were monitored using thin-layer chromatography (TLC) on silica gel(60).F₂₅₄ (Merck, Germany) and exposed to UV254 nm light. The infrared spectra were recorded using Shimadzu Specac GS 10800-R IRAffinity-1Spectrometer (ν , cm⁻¹).

CHNS microanalysis was carried out using Euro EA3000 elemental analyzer.¹HNMR of the synthesized compounds were measured on Inova show Ultra shield 500MHz. using tetramethylsilane (TMS) as an internal standard, the chemical shifts were expressed as (δ , ppm), and DMSO-*d*₆ was used as a solvent.

Chemical synthesis of ethyl picolinate (2) (Abbas et al. 2015)

An accurately weighed amount of picolinic acid (1) (10 g, 0.0812 mol) was added to 70 mL of abs. EtOH

in a 250 mL round bottom flask, and the mixture was stirred until a clear solution was obtained. The solution was cooled down to $-10\text{ }^{\circ}\text{C}$ and 3 mL of conc. H_2SO_4 was added drop wise with continuous stirring, which was accompanied by the appearance of an increasing amount of a white precipitate during the addition process. After the acid addition was completed, the white precipitate ceased to form, and the mixture was then refluxed with stirring at $80\text{ }^{\circ}\text{C}$ for 48 h. As the temperature of the mixture increased during the refluxing process, the precipitate dissolved again, and a clear solution reappeared. At the end of the reflux period, the solution was concentrated, and the residue was dissolved in 25 mL of D.W, basified with 5% NaHCO_3 , extracted thrice with 25 mL of CH_2Cl_2 , filtered over anhyd. MgSO_4 , and concentrated to yield a clear, colorless oil that was used in the next step without further purification.

Colorless oil, yield (70%), $R_f = 0.4$, ATR-FTIR (ν , cm^{-1}): 3059 Ar(CH) str, 2981, 2935, 2904 and 2873 (CH) str. of *aliph.* (CH_2) & (CH_3), 1716 str. of (C=O) (*conj* ester), 1585 (C=N) str, 1465, 1438 Ar(C=C) str, 1392, 1369 (CH_2) and (CH_3) bend, 1172 (C-O) str of ester, 748 & 705 (CH) bend. of heterocyclic.

^1H NMR (500 MHz, $\text{DMSO-}d_6$, δ =ppm): 8.71 (dd, 1H, $J=1.1$, 3.8 Hz, pyr-H), 8.04 (d, 1H, $J=7.8$ Hz, pyr-H), 7.98 (t, 1H, $J=7.8$ Hz, pyr-H), 7.63 (ddd, 1H, $J=1.1$, 4.7, 7.4 Hz, pyr-H), 4.33 (q, 2H, $J=7.1$ Hz, CH_2), 1.31 (t, 3H, $J=7.1$ Hz, CH_3).

Chemical synthesis of picolinohydrazide (3) (Abbas et al. 2015)

Ethyl picolinate compound (2) (5.6 g, 0.037 mol), and hydrazine hydrate 99.5% (an excess amount (9.0 mL, 0.185 mol), were added to 40 mL of abs. EtOH in a 250 mL round bottom flask, and the mixture was first stirred overnight at room temperature (RT), after that it was refluxed at $80\text{ }^{\circ}\text{C}$ for 12 h. It was noticed that the colorless solution changed to pale pink with time. At the end of the reflux time, half of the solvent was removed under reduced pressure and the residue was poured into ice. The precipitate was filtered and washed with ice-cold EtOH to give a product, which was recrystallized from 70% EtOH to yield compound (3).

Off-white crystals, yield (80%), m.p (98–100 $^{\circ}\text{C}$), $R_f = 0.85$, ATR-FTIR (ν , cm^{-1}): 3363 (NH) str. of *sec.* amide, 3290, 3209 (NH) str. of *prim.* amine, 3016 Ar(CH) str, 1670 str of (C=O) of amide (amide I band), 1647 (NH) bend, 1593 (C=N) str, 1566 (NH) bend. of (amide II band), 1516, 1469, 1431 Ar(C=C) str, 1246 (C-N) str, 752, 702 (CH) bend of heterocyclic.

^1H NMR (500 MHz, $\text{DMSO-}d_6$, δ =ppm): 9.89 (*br s*, 1H, NH), 8.60 (d, 1H, $J=3.8$ Hz, pyr-H), 7.96–8.0 (m, 2H, pyr-H), 7.56 (t, 1H, $J=5.5$ Hz, pyr-H), 4.61 (*br s*, 2H, NH_2).

General method for synthesis of the target compounds (4–7) (Najeh Al-Saad et al. 2019)

To a solution of compound (3) (0.5 g, 0.00364 mol) in 25 mL of abs. EtOH was added separately (A): 1-isothiocyanato-

to-4-nitrobenzene (0.657 g, 0.00364 mol), (B): 1-bromo-4-isothiocyanatobenzene (0.78 g, 0.00364 mol), (C): 1-fluoro-4-isothiocyanatobenzene (0.558 g, 0.00364 mol), (D): 1-isothiocyanato-4-methylbenzene (0.544 g, 0.00364 mol), the reaction mixture was stirred at $40\text{--}50\text{ }^{\circ}\text{C}$ for 4 h, then kept stirring overnight. Half of the solvent was removed under reduced pressure, and the residue was poured into ice. The precipitate was filtered, and washed with ice-cold EtOH to give a product, and recrystallized from 70% EtOH to yield the corresponding final target compounds (4–7).

The following target compounds were synthesized by the above-mentioned general procedure.

Synthesis of N-(4-nitrophenyl)-2-picolinoylhydrazinecarbothioamide (4)

Yellow crystals, yield (95%), m.p (210–212 $^{\circ}\text{C}$), $R_f = 0.14$, ATR-FTIR (ν , cm^{-1}): 3313 (NH) str. of *sec.* amide, 3228, 3151 (NH) str. of thioamide, 3078 Ar(CH) str, 1681 (C=O) str. of amide (amide I band), 1627 (C=N) str, 1581, 1496, 1462 Ar(C=C) str, 1556 (NH) bend. of (amide II band), 1531, 1300 *asym/sym.* str. of NO_2 group, respectively, 1261 (C-N) str, 1230 (C=S) str, 813 (Ar-*p*-substitution), 736, 698 (CH) bend. of heterocyclic.

^1H NMR (500 MHz, $\text{DMSO-}d_6$, δ =ppm): 10.87 (*br s*, 1H, C(=S) NH), 10.16 (*br s*, 1H, NH(C=S)), 10.06 (*br s*, 1H, C(=O) NH), 8.72 (d, 1H, $J=4.4$ Hz, pyr-H), 8.22–8.21 (d, 2H, $J=8.8$ Hz, Ar-H), 8.09–8.08 (m, 2H, pyr-H), 7.94 (d, 2H, $J=8.8$ Hz, Ar-H), 7.69–7.64 (m, 1H, pyr-H).

CHNS analysis: Calcd. For ($\text{C}_{13}\text{H}_{11}\text{N}_5\text{O}_3\text{S}$): C, 49.21; H, 3.49; N, 22.07; S, 10.10. Observed: C, 49.31; H, 3.66; N, 22.17; S, 10.19.

Synthesis of N-(4-bromophenyl)-2-picolinoylhydrazinecarbothioamide (5)

White crystals, yield (92%), m.p (190–193 $^{\circ}\text{C}$), $R_f = 0.26$, ATR-FTIR (ν , cm^{-1}): 3232 (NH) str of *sec.* amide, 3201, 3124 (NH) str. of thioamide, 3082 Ar(CH) str, 1654 (C=O) str of amide (amide I band), 1604 (C=N) str, 1585, 1543, 1481 Ar(C=C) str, 1570 (NH) bend. of (amide II band), 1265 (C-N) str, 1222 (C=S) str, 825 (Ar-*p*-substitution), 736, 690 (CH) bend. of heterocyclic, 720 (C-Br) str.

^1H NMR (500 MHz, $\text{DMSO-}d_6$, δ =ppm): 10.77 (*s*, 1H, C(=S)NH), 9.86 (*br s*, 2H, C(=O)NH-NH), 8.70 (d, 1H, $J=3.8$ Hz, pyr-H), 8.09–8.01 (d, 2H, Ar-H), 7.66 (dd, 1H, $J=5.5$, 6.6 Hz, pyr-H), 7.52–7.51 (d, 2H, Ar-H), 7.48 (m, 2H, pyr-H).

CHNS analysis: Calcd. For ($\text{C}_{13}\text{H}_{11}\text{BrN}_4\text{OS}$): C, 44.46; H, 3.16; N, 15.95; S, 9.13. Observed: C, 44.38; H, 3.00; N, 16.08; S, 9.32.

Synthesis of N-(4-fluorophenyl)-2-picolinoylhydrazinecarbothioamide (6)

White crystals, yield (90%), m.p (188–191 $^{\circ}\text{C}$), $R_f = 0.25$, ATR-FTIR (ν , cm^{-1}): 3290 (NH) str. of *sec.* amide, 3251, 3151 (NH) str. of thioamide, 3093 Ar(CH) str, 1651 (C=O) str. of amide (amide I band), 1616 (C=N) str, 1558 (NH) bend. of (amide II band), 1508, 1481, 1458 Ar(C=C) str, 1265 (C-N) str, 1215 (C=S) str, 829 (Ar-*p*-substitution), 762, 725 (CH) bend. of heterocyclic, 698 (C-F) str.

^1H NMR (500 MHz, DMSO- d_6 , δ =ppm): 10.75 (s, 1H, C(=S) NH), 9.75 (br s, 2H, C(=O) NH-NH), 8.71 (d, 1H, J =4.4 Hz, pyr-H), 8.09–8.02 (m, 2H, pyr-H), 7.66 (dd, 1H, J =5.5, 6.6 Hz, pyr-H), 7.46 (d, 2H, Ar-H), 7.17 (d, 2H, J =8.8 Hz, Ar-H).

CHNS analysis: Calcd. For (C₁₃H₁₁FN₄OS): C,53.78; H,3.82; N,19.30; S,11.04. Observed: C,53.74; H,3.69; N,19.52; S,11.02.

Synthesis of 2-picolinoyl-N-(p-tolyl)hydrazinecarbothioamide (7)

White crystals, yield (80%), m.p (190–192 °C), R_f = 0.28, ATR-FTIR (ν , cm⁻¹): 3290 (NH) str. of sec. amide, 3244,3201(NH) str. of thioamide, 3093,3024 Ar(CH) str, 2912,2854 (CH) str. of *aliph.*(CH₃), 1651 (C=O) str. of amide (amide I band), 1608 (C=N) str, 1589,1512,1481 Ar(C=C) str, 1550(NH) bend. of (amide II band), 1454, 1354(CH) bend. of (CH₃), 1265 (C-N) str, 1222 (C=S) str, 817 (Ar-*p*-substitution), 786,744 (CH) bend. of heterocyclic.

^1H NMR (500 MHz, DMSO- d_6 , δ =ppm): 10.72 (s, 1H, C(=S) NH), 9.67 (br s, 2H, (C=O) NH-NH), 8.70 (d, 1H, J =4.9 Hz, pyr-H), 8.09–8.04 (m, 2H, pyr-H), 7.66 (t, 1H, J =6.2 Hz, Pyr-H), 7.33 (d, 2H, Ar-H), 7.13 (d, 2H, J =8.2 Hz, Ar-H), 2.29 (s, 3H, CH₃).

CHNS analysis: Calcd. For (C₁₄H₁₄N₄OS): C,58.72; H,4.93; N,19.57; S,11.20. Observed: C,58.95; H,4.99; N,19.68; S,11.01.

Chemical synthesis of the target compounds (5A, 6A, and 7A) (Amir et al. 2007; Choi et al. 2019)

Hydrazinecarbothioamide compounds (5, 6, and 7) (0.001 mol) were separately added to 2N NaOH (6.6 mL), stirring at RT for about (15 min), a clear yellow solution appeared which was then refluxed for 3 h. The reaction mixture was cooled to RT, and then acidified with 2N HCl to pH = 3. The resulting solid was filtered and recrystallized from 70% EtOH to afford the corresponding final compounds (5A, 6A, and 7A).

The following target compounds were synthesized by the above-mentioned general procedure.

Synthesis of 4-(4-bromophenyl)-5-(pyridin-2-yl)-4H-1,2,4-triazole-3-thiol (5A)

White crystals, yield (77%), m.p (260–262 °C), R_f = 0.7, ATR-FTIR (ν , cm⁻¹): 3105 (NH) str, 3074, 3032 Ar(CH) str, 2762 (SH) str.(w), 1581,1554 (C=N) str, 1489,1458,1442 Ar(C=C) str, 1276 (C-N) str, 1234 (C=S) str, 817 (Ar-*p*-substitution), 790,763 (CH)bend. of heterocyclic, 744(C-Br) str.

^1H NMR (500 MHz, DMSO- d_6 , δ =ppm): 14.30 (s, 1H, NH), 8.37 (d, 1H, pyr-H), 7.93 (dd, 1H, J =1.6, 7.7 Hz, pyr-H), 7.90 (t, 1H, pyr-H), 7.67–7.65 (m, 2H, Ar-H), 7.43 (ddd, 1H, J =1.1, 4.8, 7.3 Hz, pyr-H), 7.31–7.29 (m, 2H, Ar-H).

CHNS analysis: Calcd. For (C₁₃H₉BrN₄S): C,46.86; H,2.72; N,16.81; S,9.62. Observed: C,46.87; H,2.96; N,16.85; S,9.48.

Synthesis of 4-(4-fluorophenyl)-5-(pyridin-2-yl)-4H-1,2,4-triazole-3-thiol (6A)

White crystals, yield (72%), m.p (229–231 °C), R_f = 0.68, ATR-FTIR (ν , cm⁻¹): 3240 (NH) str, 3093, 3070 Ar(CH) str, 2765 (SH) str.(w), 1600,1570 (C=N) str, 1539, 1508,1485 Ar(C=C) str, 1288 (C-N) str, 1222 (C=S) str, 837 (Ar-*p*-substitution), 786,750 (CH)bend. of heterocyclic, 705 (C-F) str.

^1H NMR (500 MHz, DMSO- d_6 , δ =ppm): 14.27 (s, 1H, NH), 8.36 (dd, 1H, J =1.4, 5.2 Hz, pyr-H), 7.93 (dd, 1H, J =1.1, 7.7 Hz, pyr-H), 7.88 (t, 1H, pyr-H), 7.42 (t, 1H, J =6.7 Hz, pyr-H), 7.38 (m, 2H, Ar-H), 7.29–7.28 (m, 2H, Ar-H).

CHNS analysis: Calcd. For (C₁₃H₉FN₄S): C,57.34; H,3.33; N,20.58; S,11.78. Observed: C,57.06; H,3.35; S,11.93.

Synthesis of 5-(pyridin-2-yl)-4-(p-tolyl)-4H-1,2,4-triazole-3-thiol (7A)

White crystals, yield (77%), m.p (236–239 °C), R_f = 0.49, ATR-FTIR (ν , cm⁻¹): 3086, 3028 Ar(CH) str, 2958,2924 (CH) str. of *aliph.* (CH₃), 2762 (SH) str.(w), 1585,1554 (C=N) str, 1512,1492,1460 Ar(C=C) str, 1442,1362 (CH) bend. of (-CH₃), 1234 (C-N) str, 1211 (C=S) str, 813 (Ar-*p*-substitution), 790,740 (CH)bend. of heterocyclic.

^1H NMR (500 MHz, DMSO- d_6 , δ =ppm): 14.22 (s, 1H, NH), 8.39 (m, 1H, pyr-H), 7.91 (d, 1H, pyr-H), 7.80 (d, 1H, J =7.7 Hz, pyr-H), 7.42 (dd, 1H, J =5.5, 6.6 Hz, pyr-H), 7.24 (d, 2H, J =7.7 Hz, Ar -H), 7.17 (d, 2H, J =8.2 Hz, Ar-H), 2.35 (s, 3H, CH₃).

CHNS analysis: Calcd. For (C₁₄H₁₂N₄S): C,62.66; H,4.51; N,20.88; S,11.95. Observed: C,62.62; H,4.61; N,20.66; S,12.07.

Chemical synthesis of the target compounds (5B, 6B, and 7B) (Amir et al. 2007; Choi et al. 2019)

Hydrazinecarbothioamide compounds (5, 6, and 7) (0.001 mol) were separately added to concentrated H₂SO₄ (5 mL) at 0 °C and stirred for 3 h at RT. The reaction mixture was left to stir for 3 h at RT and it was noticed that a clear yellow solution appeared. The reaction mixture was neutralized with 2N NaOH and filtered, then washed with a plenty amount of water. The compound was recrystallized with 70% EtOH to give the final compounds (5B, 6B, and 7B).

The following target compounds were synthesized by the above-mentioned general procedure.

Synthesis of N-(4-bromophenyl)-5-(pyridin-2-yl)-1,3,4-thiadiazol-2-amine (5B)

Faint pink crystals, yield (85%), m.p (244–247 °C), R_f = 0.81, ATR-FTIR (ν , cm⁻¹): 3174 (NH) str. of sec. amine, 3043 Ar(CH) str, 1612 (NH) bend, 1585,1562 (C=N) str, 1504,1489, 1431 Ar(C=C) str, 1273 (C-N) str, 825 (Ar-*p*-substitution), 779,740 (CH) bend. of heterocyclic, 713 (C-Br) str, 609 (C-S-C) str.

^1H NMR (500 MHz, DMSO- d_6 , δ =ppm): 10.76 (s, 1H NH), 8.65 (d, 1H, J =3.8 Hz, pyr-H), 8.15 (d, 1H, J =8.2 Hz,

pyr-H), 7.99 (t, 1H, $J=7.7$ Hz, pyr-H), 7.68 (d, 2H, $J=8.2$ Hz, Ar-H), 7.55 (d, 2H, $J=8.8$ Hz, Ar-H), 7.52 (t, 1H, pyr-H)

CHNS analysis: Calcd. For ($C_{13}H_9BrN_4S$): C,46.86; H,2.72; N,16.81; S,9.62. Observed: C,46.71; H,2.71; N,16.85; S,9.83.

Synthesis of *N*-(4-fluorophenyl)-5-(pyridin-2-yl)-1,3,4-thiadiazol-2-amine (6B)

Light brown crystalline powder, yield (80%), m.p (223–225 °C), $R_f=0.75$, ATR-FTIR (ν , cm^{-1}): 3217 (NH) str. of sec. amine, 3055 Ar(CH) str, 1627 (NH) bend, 1581,1562 (C=N) str, 1504,1458,1431 Ar(C=C) str, 1280 (C-N) str, 829 (Ar-*p*-substitution), 779,736 (CH) bend. of heterocyclic, 713 (C-F) str, 613 (C-S-C) str.

1H NMR (500 MHz, DMSO- d_6 , δ =ppm): 10.64 (*br s*, 1H, NH), 8.65 (d, 1H, pyr-H), 8.16 (d, 1H, $J=7.7$ Hz, pyr-H), 7.99 (t, 1H, $J=6.9$ Hz, pyr-H), 7.72 (d, 2H, Ar-H), 7.50 (t, 1H, pyr-H), 7.23 (d, 2H, $J=8.2$ Hz, Ar-H).

CHNS analysis: Calcd. For ($C_{13}H_9FN_4S$): C,57.34; H,3.33; N,20.58; S,11.78. Observed: C,57.26; H,3.27; N,20.41; S,11.58.

Synthesis of 5-(pyridin-2-yl)-*N*-(*p*-tolyl)-1,3,4-thiadiazol-2-amine (7B)

Mustard like color crystalline powder, yield (90%), m.p (221–222 °C), $R_f=0.7$, ATR-FTIR (ν , cm^{-1}): 3248 (NH) str. of sec. amine, 3012 Ar(CH) str, 2935,2885 (CH) str. of *aliph.*(CH_3), 1612 (NH) bend, 1585,1562 (C=N) str, 1516,1504 Ar(C=C) str, 1437,1381 (CH) bend. of (CH_3), 1280 (C-N) str, 837 (Ar-*p*-substitution), 740,713 (CH) bend. of heterocyclic, 617 (C-S-C) str.

1H NMR (500 MHz, DMSO- d_6 , δ =ppm): 10.53 (*s*, 1H, NH), 8.65 (d, 1H, $J=4.4$ Hz, pyr-H), 8.16 (d, 1H, $J=7.7$ Hz, pyr-H), 7.98 (t, 1H, $J=7.7$ Hz, pyr H), 7.57–7.55 (m, 2H, Ar-H), 7.49 (m, 1H, pyr-H), 7.20–7.19 (m, 2H, Ar-H), 2.29 (*s*, 3H, CH_3).

CHNS analysis: Calcd. For ($C_{14}H_{12}N_4S$): C,62.66; H,4.51; N,20.88; S,11.95. Observed: C,62.87; H,4.44; N,20.90; S,12.07.

Chemical synthesis of the target compounds (5C, 6C, and 7C) (Amir et al. 2007; Choi et al. 2019)

To a suspension of hydrazinecarbothioamide compounds (5,6, and 7) (0.001 mol) in 25 mL of EtOH, a few drops of 5N NaOH were added, with cooling and stirring at RT resulting in the formation of a clear solution. To this, iodine in potassium iodide solution (5%) was added drop wise with stirring till the color of iodine persisted at RT, and a light brown precipitate appeared. The reaction mixture was then refluxed for 6 h on a water bath, then kept stirring at RT overnight. It was then concentrated, cooled, and the solid separated out was filtered, dried, and recrystallized from 70% EtOH to the corresponding final compounds (5C, 6C and 7C).

The following target compounds were synthesized by the above-mentioned general procedure.

Synthesis of *N*-(4-bromophenyl)-5-(pyridin-2-yl)-1,3,4-oxadiazol-2-amine (5C)

Light brown crystals, yield (75%), m.p (282–285 °C), $R_f=0.73$, ATR-FTIR (ν , cm^{-1}): 3248 (NH) str. of sec. amine, 3070 Ar(CH) str, 1612 (NH) bend, 1581,1546 (C=N) str, 1489,1458,1438 Ar(C=C) str, 1292 (C-O-C) str. of oxadiazole, 1234 (C-N) str, 817 (Ar-*p*-substitution), 786,736 (CH) bend. of heterocyclic, 721 (C-Br) str.

1H NMR (500 MHz, DMSO- d_6 , δ =ppm): 11.04 (*s*, 1H, NH), 8.74 (d, 1H, $J=3.8$ Hz, pyr-H), 8.11 (d, 1H, $J=7.7$ Hz, pyr H), 8.09 (t, 1H, pyr-H), 7.56–7.62 (m, 5H, Ar and pyr-H).

CHNS analysis: Calcd. For ($C_{13}H_9BrN_4O$): C, 49.23; H,2.86; N,17.67. Observed: C,49.20; H,2.76; N,17.75.

Synthesis of *N*-(4-fluorophenyl)-5-(pyridin-2-yl)-1,3,4-oxadiazol-2-amine (6C)

Light brown crystalline powder, yield (80%), m.p (242–245 °C), $R_f=0.66$, ATR-FTIR (ν , cm^{-1}): 3259 (NH) str. of sec. amine, 3078 Ar(CH) str, 1620 (NH) bend, 1589,1558 (C=N) str, 1504,1458,1438 Ar(C=C) str, 1292 (C-O-C) str. of oxadiazole, 1249 (C-N) str, 829 (Ar-*p*-substitution), 786,736 (CH) bend. of heterocyclic, 717 (C-F) str.

1H NMR (500 MHz, DMSO- d_6 , δ =ppm): 10.89 (*s*, 1H, NH), 8.73 (d, 1H, $J=4.9$ Hz, pyr-H), 8.10 (d, 1H, $J=8.2$ Hz, pyr-H), 8.02 (t, 1H, pyr-H), 7.66–7.63 (d, 2H, Ar-H), 7.57 (dd, 1H, $J=5.5, 6.6$ Hz, pyr-H), 7.24 (t, 2H, $J=8.8$ Hz, Ar-H).

CHNS analysis: Calcd. For ($C_{13}H_9FN_4O$): C,60.94; H,3.54; N,21.87. Observed: C, 60.99; H, 3.37; N, 21.64.

Synthesis of 5-(pyridin-2-yl)-*N*-(*p*-tolyl)-1,3,4-oxadiazol-2-amine (7C)

Faint pink crystalline powder, yield (85%), m.p (219–222 °C), $R_f=0.46$, ATR-FTIR (ν , cm^{-1}): 3263 (N-H) str. of sec. amine, 3062 Ar(CH) str, 2916,2858 (CH) str. of *aliph.*(CH_3), 1608 (NH) bend, 1581,1558 (C=N) str, 1543, 1516,1458 Ar(C=C) str, 1438,1345 (CH) bend. of (CH_3), 1292(C-O-C) str. of oxadiazole, 1249 (C-N) str, 817 (Ar-*p*-substitution), 767,721 (CH) bend. of heterocyclic.

1H NMR (500 MHz, DMSO- d_6 , δ =ppm): 10.72 (*br s*, 1H, NH), 8.72 (d, 1H, $J=4.4$ Hz, pyr-H), 8.09 (d, 1H, $J=8.2$ Hz, pyr-H), 8.00 (t, 1H, $J=7.7$ Hz, pyr-H), 7.56–7.51 (m, 3H, Ar and pyr-H), 7.18 (d, 2H, $J=8.2$ Hz, Ar-H), 2.27 (*s*, 3H, CH_3).

CHNS analysis: Calcd. For ($C_{14}H_{12}N_4O$): C,66.65; H,4.79; N,22.21. Observed: C,66.53; H,5.02; N,22.25.

The synthesis of the target compounds (4–7) and their intermediates is depicted in (Fig. 1).

Biological analysis

Cell culture

Human A549 lung cancer cell line was cultured in Ham's F-12K (Kaighn's) medium (Gibco, USA) supplemented with 10% fetal bovine serum (FBS; Capricorn Scientific, Germany), human MCF-7 breast cancer cells were cultured

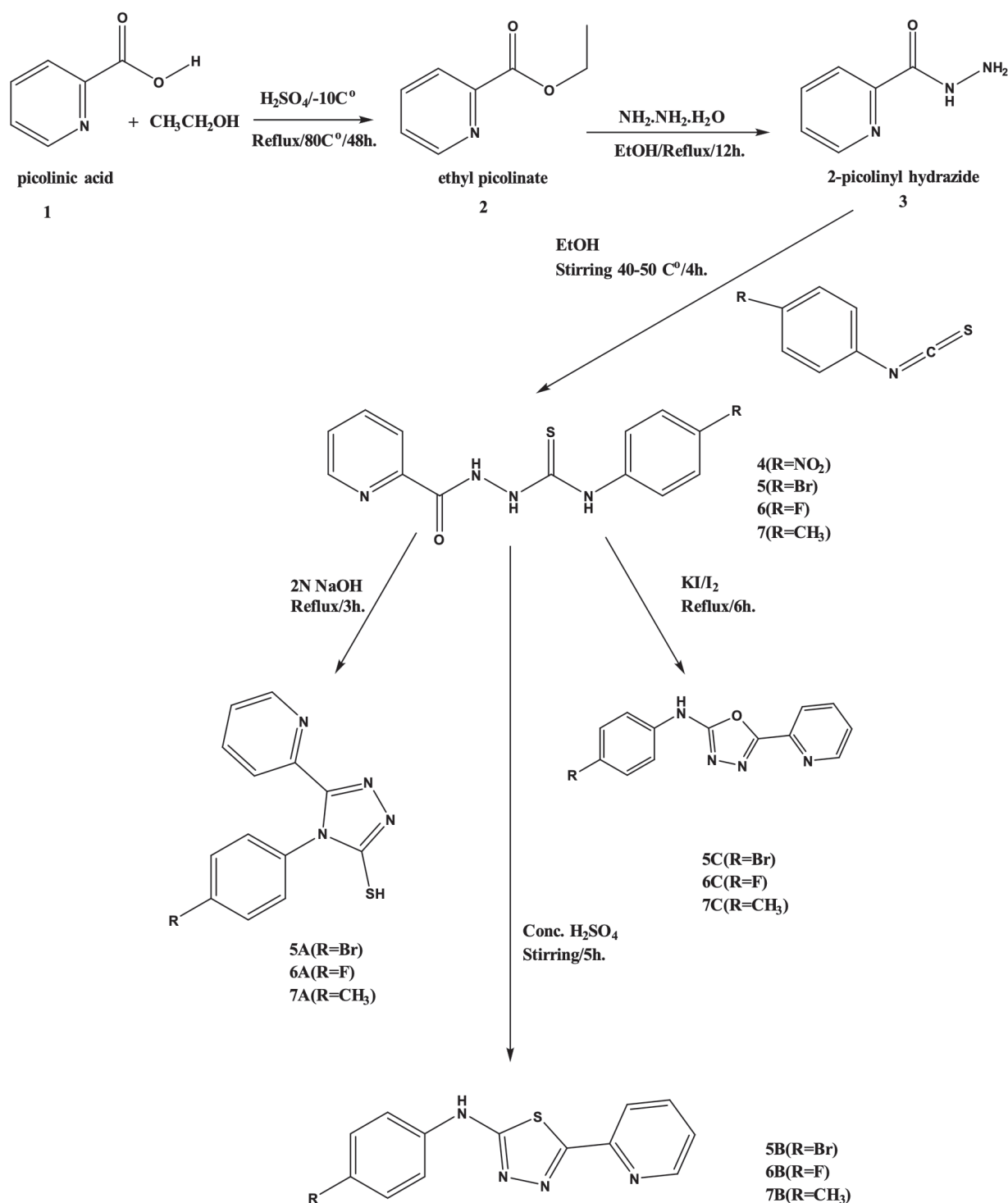


Figure 1. Synthesis of the target compounds (4–7).

in RPMI-1640 medium (Euroclone, Italy) supplemented with 10% FBS, the mammary non-tumorigenic MCF10A cell line was cultured in DMEM/F12 (Gibco, USA) supplemented with 5% horse serum (Invitrogen, USA), EGF (20 ng/mL, Sigma), hydrocortisone (0.5 mg/mL, Sigma), cholera toxin (100 ng/mL, Sigma), and insulin (10 µg/mL, Sigma), and human normal white blood cells (WBC) were isolated from peripheral blood after lysis of erythrocytes with ammonium chloride (Dagur and McCoy, 2015) and cultured in RPMI-1640 medium supplemented with 5%

FBS. Trypsin-EDTA (Lonza, Switzerland) was routinely used for subcultures. Cell growth was accomplished at 37 °C in a 5% carbon dioxide and 95% air atmosphere.

***In vitro* cytotoxicity MTT assay**

Cytotoxicity of the different picolinic acid derivatives (4–7) against different cell lines (A549, MCF-7 and MCF10A), and WBC was assessed using the MTT (Tetrazolium Salt Reduction) test (Mosmann 1983; Fotakis and Timbrell 2006). Compound stock solutions were prepared with 10%

DMSO; the final concentration of DMSO in the media did not exceed 0.1%. Seven concentrations (0.5, 1, 2.5, 5, 10, 25 and 50 µg/mL) were prepared for each compound in the growth media. Viable cells (50,000) were added to each well of a 96-well tissue culture plate containing growth medium supplemented by FBS. Cells were kept in a humidified 5% CO₂ incubator at 37 °C for 24 h. The next morning, various concentrations were added, and the cells were incubated for 24 h, 48 h and 72 h. Freshly prepared MTT salt (3-(4,5-dimethylthiazol-2-yl)-2,5-diphenyltetrazolium bromide; Sigma) (5 mg/mL) was then added to each well at a final concentration of 0.5 µg/µL. The plates were incubated for 4 h, and the formation of formazan crystals was verified using an inverted microscope. Equal volume of 1:1 (200 µL) DMSO and isopropanol mixture was added to each well and incubated for 30–45 min. Inhibition of cell growth induced by the different compounds was monitored by measuring the absorbance of each well at 570 nm by using Biotek Synergy HT Multi-Mode Microplate Reader (VT, USA). Percent growth was determined using the following equation: Growth (%) = OD-treated/OD-treated vehicle control × 100%. The “dose-effect” curve was also used to calculate the concentration that caused 50% growth inhibition (GI₅₀) by linear interpolation from a semi-log dose response curve. The test was repeated three times in triplicate.

Detection of apoptosis

Apoptosis was recorded by visual analysis of apoptotic nuclei after staining with DAPI. Cells were plated on sterile glass cover slips for 24 h. Thereafter, the cells were treated with the various compound(s) at the GI₅₀ concentration. Cells were fixed with 4% paraformaldehyde (Sigma, USA) in phosphate buffered saline (PBS) for 45 min. Cells were then washed 3 times 3 min each with PBS. Cells were then mounted with Prolong Gold antifade containing DAPI (Invitrogen). Images were captured using 100× NA 1.3 objective on Nikon Eclipse Ti-E microscope with a CCD camera and operated by NIS-Elements software. Furthermore, DNA fragmentation was analyzed by agarose gel electrophoresis. Briefly, DNA from control and treated cells was extracted as per the manufacturer instructions (Wizard Genomic DNA Purification, Promega). The DNA samples were electrophoresed on a 1.5% agarose gel containing 5 µL/100 mL RedSafe nucleic acid staining solution (iNtRON Biotechnology, South Korea). The gel was examined and photographed using ultraviolet gel documentation system (FluorChem R System, Oxford, UK).

Quantitative reverse transcription polymerase chain reaction (qRT-PCR)

The quantity of caspase 3, caspase 4, caspase 8, caspase 9 mRNA was determined by qRT-PCR (Tahtamouni et al. 2018; Nawasreh et al. 2020). Total RNA from vehicle-treated control and GI₅₀-treated cells was extracted according to the manufacturer instructions (Total RNA Isolation System, Sigma-Aldrich, USA). After RNA extraction, cDNA was prepared using Power cDNA synthesis kit (iNtRON Biotechnology, South Korea). Amplification of target cDNA for

apoptosis markers and β-actin (as a normalization gene) was completed using KAPA SYBRFAST qPCR Kit Master Mix (KAPA BIOSYSTEMS, USA) on Line Gene 9680 BioGR instrument. cDNA (5 µL aliquots) was mixed with 1 µL of forward primer (25X), 1 µL reverse primer (25X) (Van Geelen CM et al. 2010; Yaoxian et al. 2013), 5.5 µL nuclease free water and 12.5 µL master mix. All experiments were performed in triplicate. The relative mRNA quantity was normalized to β-actin.

Western blot analysis

Control and GI₅₀-treated cells were washed 3 times with cold PBS, and then lysed with protein lysis buffer [10% sodium dodecyl sulfate (SDS), 1 M Tris buffer pH 7.5, 1 M sodium fluoride (NaF), 1M dithiothreitol (DTT), 0.1 M ethylene glycol tetra-acetic acid (EGTA) and distilled water] on ice. The cell lysate was collected and boiled for 5 min and sonicated. Aliquots of lysates were diluted in 4× SDS-PAGE sample buffer (0.5 M Tris-HCl pH 6.8, 2% SDS, 20% glycerol, 20% 2-mercaptoethanol and 0.16% bromophenol blue) and proteins were resolved by electrophoresis on 10% or 12.5% SDS-polyacrylamide gels. Proteins were transferred onto nitrocellulose membranes and were blocked using 2% (w/v) BSA in Tris-buffered saline (TBS), and incubated overnight at 4 °C with the different primary antibodies: mouse monoclonal anti-caspase 3 (1:500; Invitrogen, USA), mouse monoclonal anti-caspase 9 (1:1000; Invitrogen, USA), rabbit polyclonal anti-caspase 4 (1:1000; Invitrogen, USA), mouse monoclonal anti-caspase 8 (1:1000; Invitrogen, USA), rabbit polyclonal anti-smac/DIABLO (1:1000; R&D Systems, Germany), mouse GAPDH (1:6000; CHEMICON, USA), rabbit monoclonal phospho-eukaryotic initiation factor-2 (p-EIF-2) (1:2000; Cell Signaling Technology, USA) rabbit polyclonal anti-tubulin (1:3000; abcam, USA), diluted in 1% BSA in TBS containing 0.05% Tween 20. After washing and incubation with appropriate secondary antibodies conjugated to IRDye 680 or 800 nm fluorescent dyes, the membranes were washed, and the bands were visualized on FluorChem R system (Oxford, UK). Signals were quantified using AlphaView software (ProteinSimple, USA).

Cytochrome c release apoptosis assay

5×10⁷ control and GI₅₀-treated cells were collected by centrifugation and washed with ice cold PBS at 2,900 rpm for 5 min and re-suspended with 1X cytosolic extraction buffer mix containing dithiothreitol (DTT) and protease inhibitors. The cells were incubated on ice for 10 min, homogenized and centrifuged at 3,100 rpm for 10 min. The supernatant was centrifuged again at 12,000 rpm for 30 min to obtain the cytosolic fraction, while the pellet was resuspended in mitochondrial extraction buffer to get mitochondrial fraction (Cytochrome c Release Apoptosis Assay Kit, Abcam, USA).

EGFR kinase inhibitory assay

The EGFR(T790M/L858R) Kinase Assay Kit (BPS Bioscience, USA) was used to assess the inhibitory activity of the

cytotoxic compound(s) against EGFR kinase. The reaction process was halted by addition of detection reagent (Kinase-Glo Max reagent, Promega). The remaining activity of EGFR kinase was detected by measuring chemiluminescence. The effective concentration that inhibits 50% of EGFR kinase activity (EC_{50}) was calculated from the compounds' concentration versus EGFR kinase remaining activity curve. Each experiment was performed in duplicates.

Statistical analysis

Results are expressed as mean \pm SEM. Statistical analysis was performed using GraphPad Prism version 5.0 (GraphPad Software, San Diego, CA, USA). The student's t-test was used to test for significant differences between means. p value ≤ 0.05 was considered significant.

Molecular docking study

In order to identify the molecular targets, the newly synthesized compounds (4–7) would eventually work on, and in order to compare them with several other ligands, and to ascertain the pharmacophoric functionality that would allow binding with critical amino acid(s) in a target site, target site selection was done by (<https://www.rcsb.org/>) protein data bank. The tested compounds were practically examined against a large number of binding sites, and the results were used to identify relevant proteins for docking studies. After selecting a protein for the target location, several processes were put forth to gain an understanding of the molecular binding modes of the tested compounds within the pocket of the epidermal growth factor receptor tyrosine kinase (ATP binding site of EGFR kinase) using the MOE 2015 Software. The binding sites were generated by co-crystallizing the ligand within the crystal protein (PDB code: 1M17) (Khalil et al. 2015). Water molecules were first removed from the complex, and then crystallographic disorders, and unfilled valence atoms were corrected using protein report, and utility, and clean protein options. CHARMM and MMFF94 force fields were used to reduce protein energy. Using a fixed atom constraint, a protein's rigid binding site was obtained. The essential amino acids in proteins were identified and prepared for docking. The Chem-Bio Draw Ultra14.0 was used to create 2D structures of the tested compounds, which would then be saved in MDL-SD format. The saved file was opened in the MOE 2015 software, and the 3D structures were protonated, and energy was kept to a minimum by using a 0.05 Å RMSD. CHARMM force field. The minimized structures were then ready for docking using a prepared ligand protocol (El-Helby et al. 2019).

Results and discussion

In vitro biological evaluation

Compound 5 causes cytotoxicity in human A549 lung cancer cells

The cytotoxicity of 13 different picolinic acid derivatives (4, 5, 5A, 5B, 5C, 6, 6A, 6B, 6C, 7, 7A, 7B, and 7C) against

two human cancer cell lines, A549 and MCF-7 was explored. According to the findings, compound 5 was the only one demonstrating cytotoxicity against A549 lung cancer cells ($GI_{50} = 35.1 \mu\text{g/mL}$ (99.93 μM) after 48 h of treatment). None of the remaining compounds were effective against the A549 lung carcinoma cells, most of them showed an average of 25% maximum growth inhibition after 72 h of treatment with the highest concentration (50 $\mu\text{g/mL}$), while compounds 4, 5C, and 6 showed an average of 43% growth inhibition. However, none of the different compounds exhibited cytotoxic activities against MCF7 breast cancer cells, with the majority of the compounds showing an average of 25% maximum growth inhibition after 72 h of treatment with the highest concentration (50 $\mu\text{g/mL}$), while compounds 4 and 5 showed an average of 42% growth inhibition.

Compound 5 cytotoxicity is cancer-cell specific

The cytotoxicity of compound 5 was tested against two non-cancer cell types, the non-tumorigenic mammary MCF10A cells, and WBC (Fig. 2). The findings showed that compound 5 did not exert cytotoxicity in normal cells even after 72 h of treatment at the highest compound concentration tested (50 $\mu\text{g/mL}$) (Fig. 2). As a result, compound 5's toxic effect is considered cancer-cell specific. It is worth mentioning that compound 5 showed growth increment in these cells (more in WBC than in MCF10A), although insignificant when compared to control untreated cells (Fig. 2). One explanation is that since MTT assay depends on the activity of mitochondrial dehydrogenases, compound 5 might have interfered with enzyme activity without affecting cell proliferation, another explanation is the natural variation of cellular metabolism (Jaszczyszyn and Gasiorowski 2008), however, exploration of this was beyond the scope of the current work.

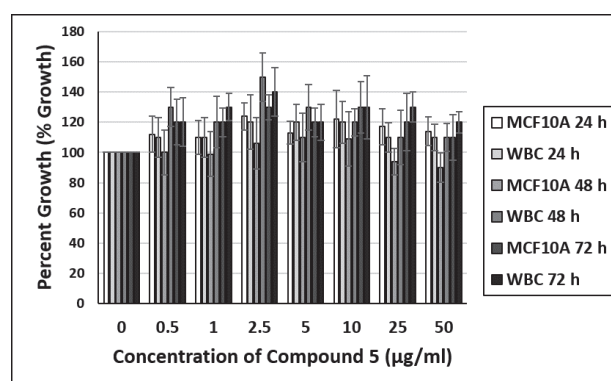


Figure 2. The MTT (3-(4,5-dimethylthiazol-2-yl)-2,5 diphenyltetrazolium bromide) assay results for compound 5 against MCF10A cells, and white blood cells (WBC) after 24, 48 and 72 h of treatment.

Cytotoxicity of compound 5 is attributed to induction of apoptosis

The results presented in Fig. 3 revealed that compound 5 induced apoptosis in A549 lung cancer cells, as evident by

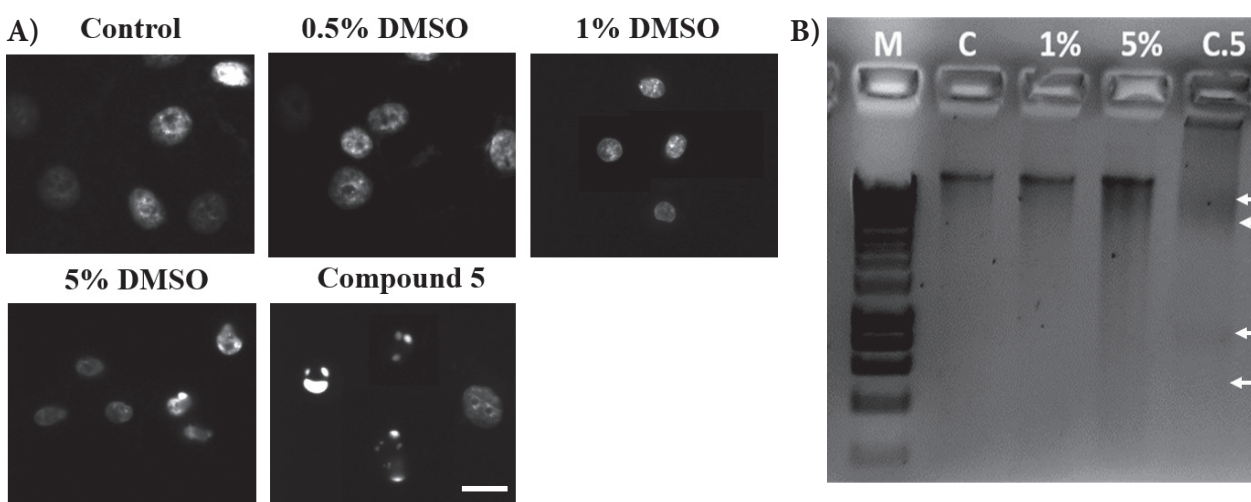


Figure 3. Compound 5 induces apoptosis in A549 lung cancer cells. **A)** Fluorescence images of A549 lung cancer cells showing fragmented nuclei after DAPI staining. Scale bar: 10 μ m, **B)** Detection of DNA fragmentation by agarose gel electrophoresis. Cells were treated and genomic DNA was extracted and electrophoresed on 1.5% agarose gels. M: DNA molecular weight marker; C: vehicle-treated control cells; 1%: 1% DMSO-treated cells; 5%: 5% DMSO-treated cells; C.5: Compound 5-treated cells. Arrows indicate DNA fragments. Three experiments were performed with similar results.

fragmented nuclei after DAPI staining (Fig. 3A), and agarose gel electrophoresis (Fig. 3B). Cells treated with 0.5% or 1% DMSO exhibited no cytotoxicity, however, cells treated with 5% DMSO showed shrunken nuclei and sporadic nuclei fragmentation (Fig. 3A) which did not cause overall DNA fragmentation (Fig. 3B).

Compound 5 induction of apoptosis is dependent on activation of caspase 3, 4, and 9

To investigate the role of caspase activation in inducing the apoptotic cell death by compound 5, the mRNA levels of caspase 3, caspase 4, caspase 8 and caspase 9 were evaluated by qRT-PCR (Fig. 4A), and their activation (cleavage) was assessed using Western blotting (Fig. 4B). When A549 lung cancer cells were treated with 0.5% or 1% DMSO, there was no increase in the mRNA levels of any of the caspases (Fig. 4A) as compared to the vehicle-treated control cells, or their activation (Fig. 4B). On the other hand, treating these cells with 5% DMSO led to a significant increase in caspase 3 and caspase 9 mRNA levels (Fig. 4A), and their activation (Fig. 4B), while compound 5 treatment increased the mRNA levels of caspase 3 (insignificantly), caspase 4 and caspase 9 (significantly) as compared to control cells (Fig. 4A), as well as their activation (Fig. 4B). None of the treatments significantly affected caspase 8 mRNA level or induced its activation (Fig. 4).

Compound 5 induces apoptosis through the ER stress pathway

Since compound 5 activated caspases 3, 4 and 9 (Fig. 4), we tried to look into the upstream signaling pathway(s). Caspase 3 is activated downstream of caspase 9 which is involved in the intrinsic pathway, cytochrome c release from the mitochondria is a hallmark of this pathway (Wang et al. 1999). Furthermore, caspase 9 can be acti-

vated downstream of caspase 4 that is activated by the ER stress pathway, the hallmarks of which are increased phosphorylation of the eukaryotic translation initiation factor 2 (eIF2), and the release of Smac/DIABLO into the cytosol (d'Azzo et al. 2006). Figure 5 showed that compound 5 treatment did not trigger the release of cytochrome c from the mitochondria to the cytosol as compared to vehicle-treated control cells (Fig. 5A, B). However, compound 5-treated cells demonstrated enhanced release of smac/DIABLO into the cytosol (Fig. 5A, B). Moreover, both compound 5 and thapsigargin (specific sarco/endoplasmic reticulum Ca^{2+} ATPase (SERCA) inhibitor) enhanced the phosphorylation of eIF2 (Fig. 5C), reflecting the activation of the ER stress pathway.

Compound 5 inhibits EGFR when analyzed by molecular docking but not when studied in vitro

The CDOCKER protocol was used for the molecular docking procedure. CDOCKER is a grid-based molecular docking method that docks ligands into receptor binding sites that used a CHARMM-based molecular dynamics (MD) scheme. Mostly during refinement, the receptor was kept rigid, while the ligands were allowed to be flexible. Each molecule was given the opportunity to take seven distinct interactions with the protein. The docking scores (-CDOCKER interaction energy) of the best-fitting poses with the active site, the EGFR kinase's ATP binding site, was recorded (Table 1). This was used to anticipate the suggested binding mode, affinity, preferred orientation of each docking pose, and binding free energy (ΔG) of the compounds tested with EGFR kinase's ATP binding site.

For EGFR tyrosine kinase, the key binding site consists of the amino acids Asp776, Thr766, leu694, Cys773, Gly772, and Val702 (Patel and Narechania 2018). The prototype binding mode for each line of synthesized com-

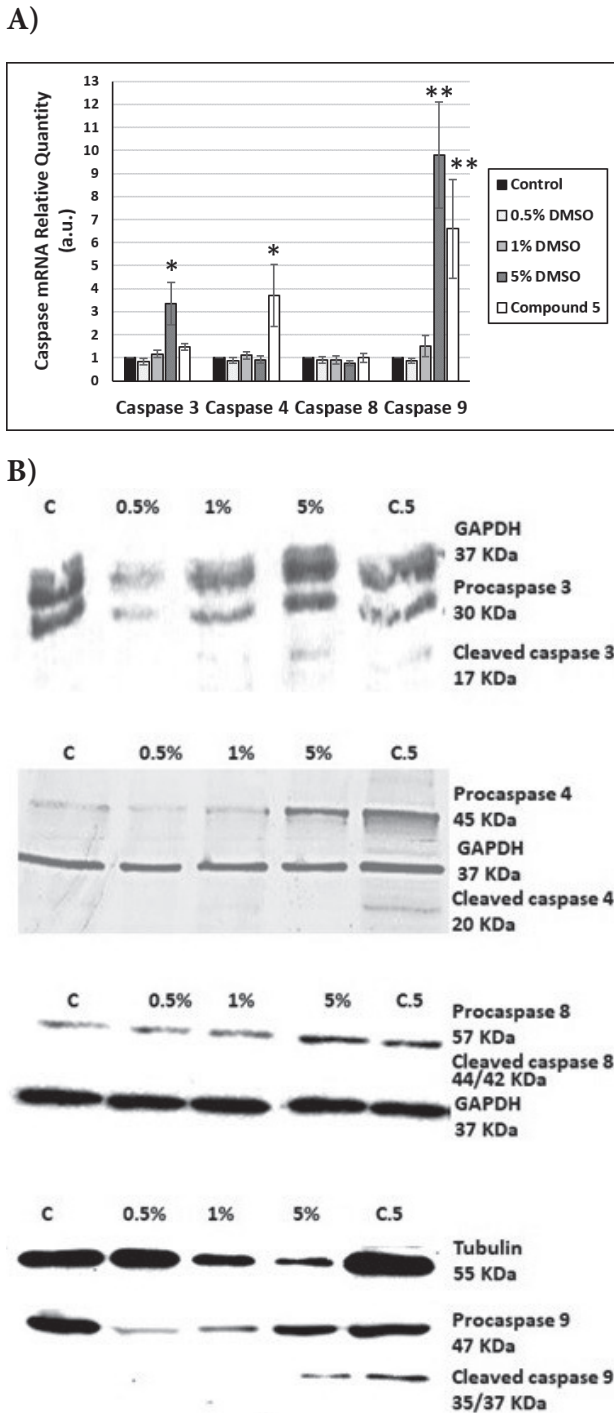


Figure 4. Compound 5 causes caspase activation. **A)** qRT-PCR analysis of caspase 3, 4, 8 and 9 mRNA in compound 5-treated cells (GI_{50}) as compared to vehicle-treated control cells [set as 1 arbitrary unit (a.u.)]. Values were normalized to β -actin. Scale bars: mean \pm SEM of three independent experiments performed in triplicates. * $p < 0.05$, ** $p < 0.01$ compared to vehicle-treated control cells, **B)** Representative Western blots showing cleavage “activation” of procaspase 3 to the active form p17, procaspase 4 to the active form p20, and procaspase 9 to the active forms p35/p37. C: vehicle-treated control cells; 0.5%: 0.5% DMSO-treated cells; 1%: 1% DMSO-treated cells; 5%: 5% DMSO-treated cells; C.5: Compound 5-treated cells. The experiment was repeated three times.

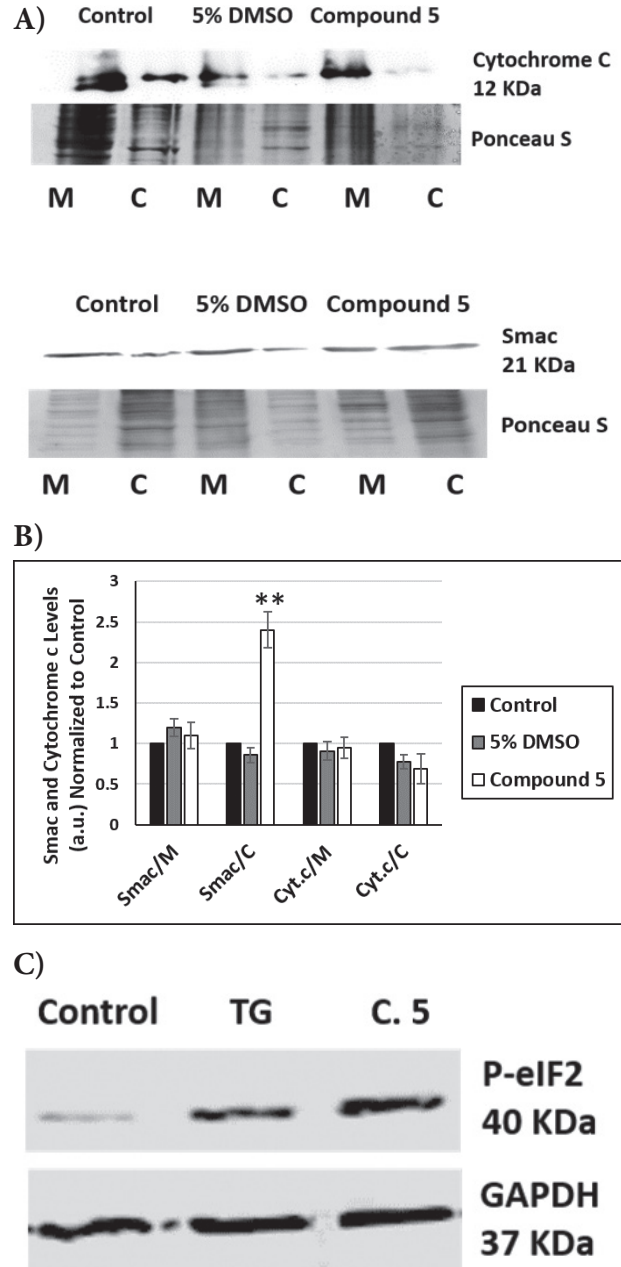


Figure 5. Compound 5 induces the ER-mediated apoptosis. **A)** Representative Western blot showing the enhanced release of Smac/DIABLO but not cytochrome c from the mitochondria (MF) into the cytosol (CF) of compound 5-treated A549 lung cancer cells (GI_{50}). Equal protein loading was controlled by staining membranes with Ponceau S (a representative section of the stained membrane is shown). The experiment was repeated three times and the corresponding quantification is shown in **B)** Quantification of smac/DIABLO and cytochrome C levels in vehicle-treated control A549 cells and cells treated with GI_{50} amount of compound 5 or 5% DMSO as a negative control. M: mitochondria fraction; C: cytosol fraction. Scale bars: mean \pm SEM of three independent experiments. ** $p < 0.01$ compared to vehicle-treated control cells, **C)** Representative Western blot showing the induction of phosphorylation of eukaryotic initiation factor-2 (eIF-2) in A549 cells treated with GI_{50} amounts of compound 5. For comparison purposes, thapsigargin (TG), an ER stress-causing drug was used ($3 \mu M$, 2 h) as a positive control. The experiment was repeated three times.

Table 1. Docking scores (ΔG , kcal/mol) of the tested compounds against (EGFR Kinase) target site PDB ID: 1M17.

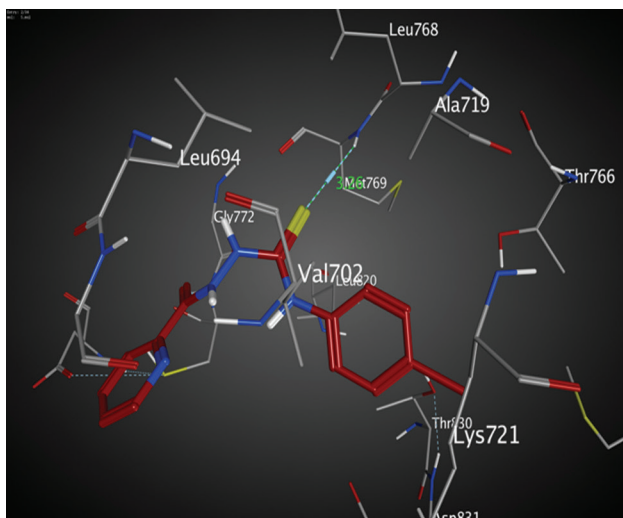
Comp.	Bonds NO.		Score (ΔG) kcal/mol	RMSD value/ $^{\circ}$ A	E-place
	H.B	pi			
4	1	–	-5.49	2.18	-63.43
5	1	–	-5.90	1.69	-70.81
5A	1	2	-5.52	2.14	-51.75
5B	1	2	-5.40	1.74	-62.23
5C	2	1	-5.74	2.58	-64.46
6	1	1	-5.45	3.08	-70.28
6A	1	1	-5.89	2.24	-69.22
6B	1	–	-6.06	1.44	-61.70
6C	2	–	-5.96	1.23	-57.89
7	1	1	-5.06	3.34	-59.31
7A	1	1	-6.05	2.04	-64.00
7B	1	2	-5.07	3.13	-58.98
7C	–	1	-5.68	1.74	-52.84
Erlotinib	1	1	-5.90	2.36	-80.69

pounds was as follows: The binding mode of compound 5 exhibited an energy binding of -5.90 kcal/mol. The *thiourea* linker formed a hydrogen bonding with Met769 with a distance of 3.26 $^{\circ}$ A (Fig. 6A). Compound 7A exhib-

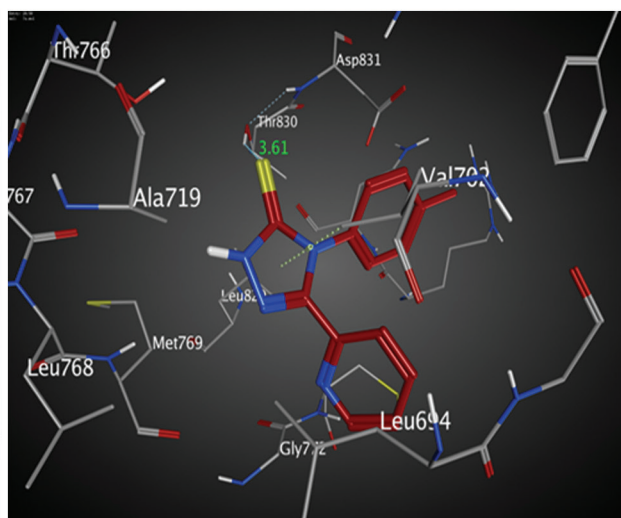
ited an energy binding of -6.05 kcal/mol. The sulfur group at triazole-3-thione ring formed hydrogen bonding with Thr830 (3.61 $^{\circ}$ A), in addition, another hydrophobic interaction formed with Val702 (Fig. 6B). The proposed binding mode of compound 6B displayed an energy binding of -6.06 kcal/mol. The azo group at thiadiazole ring formed one hydrogen bond with Met769, at a distance of 2.20 $^{\circ}$ A (Fig. 6C). Finally, compound 6C, showed an energy binding of -5.96 kcal/mol. The azo group at oxadiazole moiety formed hydrogen bonding with Lys721 at a distance of 2.31 and 2.44 $^{\circ}$ A (Fig. 6D).

The higher the score of ΔG the greater the affinity of the tested compound for EGFR binding site, which results in higher toxicity towards cancer cells (including the low EGFR-expressing MCF-7 cells) compared to healthy cells which express low levels of EGFR (Rimawi et al. 2010). However, when compound 5 was assessed for its in vitro EGFR kinase inhibition effects, compound 5 did not show EGFR kinase inhibitory activity in contrast to the results of the molecular docking studies.

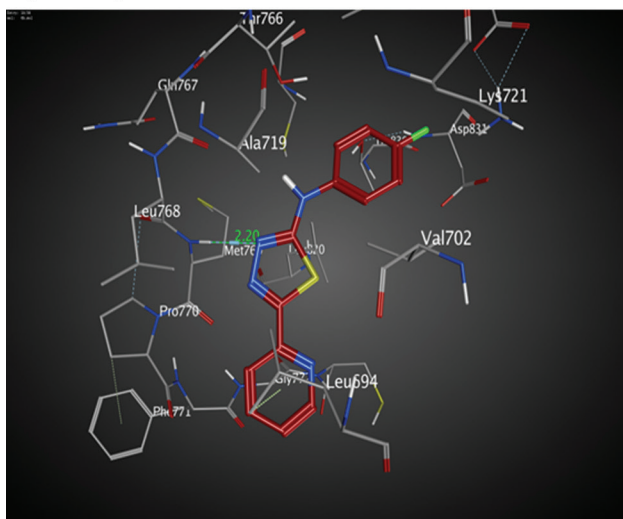
A) Comp. 5



B) Comp. 7A



C) Comp. 6B



D) Comp. 6C

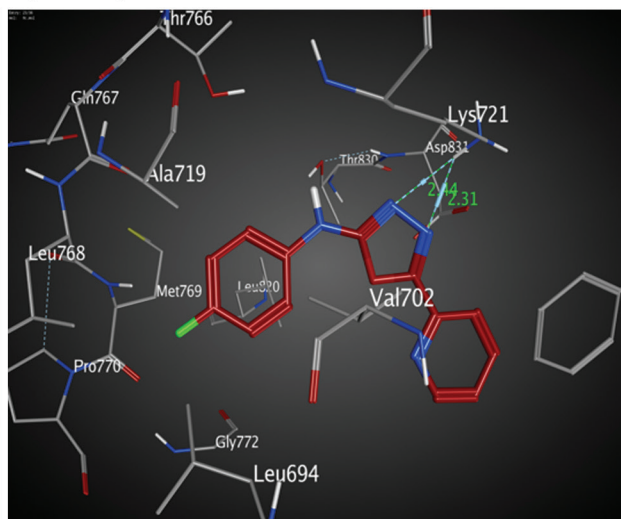
**Figure 6.** 3D View of the target compounds (5, 7A, 6B and 6C) docked against ATP binding site of EGFR kinase.

Table 2. Physicochemical properties of the synthesized compounds.

Comp.	Clog p	n. H-bond acceptors	n. H-bond donors	n. rotatable bonds	n. violation	TPSA
4	0.92	4	3	7	0	143.96
5	2.25	2	3	6	0	98.14
5A	3.25	2	1	2	0	78.59
5B	3.38	3	1	3	0	78.94
5C	2.85	4	1	3	0	63.84
6	1.95	2	3	6	0	98.14
6A	2.93	3	1	2	0	78.59
6B	3.06	4	1	3	0	78.94
6C	2.54	5	1	3	0	63.84
7	1.96	2	3	6	0	98.14
7A	2.94	2	1	2	0	78.95
7B	3.09	3	1	3	0	78.94
7C	2.56	4	1	3	0	63.84
Erlotinib	3.23	6	1	10	0	74.73

Molecular docking studies are used to aid researchers in obtaining possible candidates for protein-ligand binding, however, these studies are theoretical since they are based on algorithms and programs rather than experimental work. It has been reported that the accuracy of docking studies can vary between 0–92% (Chen 2014). Our recently published work (Abbas et al. 2021) showed that compound (4C) that gave a low ΔG score (when compared to the other tested compounds including erlotinib) in EGFR kinase molecular docking studies was the most potent cytotoxic compound and its cytotoxicity was mediated via inhibition of EGFR kinase when studied *in vitro*.

Although molecular docking studies have several shortcomings such as choosing an inaccurate binding site of the target protein, screening using unsuitable database, or inconsistency between docking results and *in vitro* experimental results (the current work is a good example), it helps researchers in solving the problem of choosing samples for *in vitro* protein-ligand experiments (Huang and Zou 2010).

Physicochemical properties

The physical characters of drugs play a key role in their molecular activity. One of these parameters is the calculated partition coefficient (Clog p) which predicts

Table 3. Predicted ADMET analysis for the designed compounds.

Comp.	BBB	HIA	CYTP450 3A4	CYP2D6	CYP2C9	PPB
4	No	40.5	Non-inhibitor	Non-inhibitor	Non-inhibitor	100%
5	No	93.07	Inhibitor	Non-inhibitor	Inhibitor	100%
5A	No	96.7	Non-inhibitor	Non-inhibitor	Inhibitor	91.8%
5B	No	96.3	Inhibitor	Inhibitor	Inhibitor	90.3%
5C	Yes	95.92	Non-inhibitor	Non-inhibitor	Non-inhibitor	91.8%
6	No	91.63	Non-inhibitor	Non-inhibitor	Non-inhibitor	100%
6A	No	96.8	Non-inhibitor	Non-inhibitor	Non-inhibitor	87.8%
6B	No	96.6	Inhibitor	Inhibitor	Non-inhibitor	86.3%
6C	Yes	95.7	Non-inhibitor	Non-inhibitor	Non-inhibitor	80.4%
7	No	91.9	Non-inhibitor	Non-inhibitor	Non-inhibitor	99.0%
7A	No	96.80	Non-inhibitor	Non-inhibitor	Inhibitor	92.5%
7B	No	96.6	Inhibitor	Inhibitor	Inhibitor	91.1%
7C	Yes	95.8	Inhibitor	Non-inhibitor	Non-inhibitor	96.5%
Erlotinib	Yes	96.04	Inhibitor	Inhibitor	Inhibitor	93.1%

drug movement patterns in the human body. All of the target compounds have (Clog p) less than <5 and are in clear violation of Lipinski rule of five. The topological polar surface area (TPSA) of a compound indicates the surface belonging to polar atoms in the compound. An increased TPSA is associated with lower membrane permeability, and compounds with higher TPSA seemed to be better p-glycoprotein substrates (responsible for drug efflux from cell). Once comparing the compounds, lower TPSA reported to be much more desirable for drug-like property (Table 2) (Nisha et al. 2016; Hmood and Mahmood 2020).

In silico ADMET and carcinogenicity analysis

The online admetSAR chemformatics software was also used to investigate the ADMET features, and the profile of the synthesized compounds, in order to identify the potential and safer drug candidates, and to filter compounds that are the most likely to fail in subsequent stages of drug development due to unfavorable ADMET properties. The anticipated ADMET analysis of the target compounds is shown in (Table 3).

The target compounds were reported to have better human intestinal absorption, except for compound 4 that possessed HIA value of 40.5 (Eissa et al. 2018). It can be deduced that some of these molecules are capable of cross-

Table 4. The carcinogenicity prediction of the synthesized compounds.

Comp.	Ames test	Carcinogen on mouse	Carcinogen on rat	HERG inhibitor	Carcinogenicity	TA100-NA
4	Mutagen	Negative	Positive	Medium risk	0	Positive
5	Mutagen	Negative	Positive	Medium risk	0	positive
5A	Mutagen	Positive	Positive	Medium risk	0	positive
5B	Mutagen	Negative	positive	Medium risk	1*	Negative
5C	Mutagen	Positive	positive	Medium risk	0	Negative
6	Mutagen	Negative	positive	Medium risk	0	positive
6A	Mutagen	Positive	positive	Medium risk	0	positive
6B	Mutagen	Positive	positive	Medium risk	1*	Negative
6C	Mutagen	Positive	positive	Medium risk	0	Negative
7	Mutagen	Positive	Negative	Medium risk	0	Positive
7A	Mutagen	Negative	Negative	Medium risk	1*	Negative
7B	Mutagen	Negative	Negative	Medium risk	0	Negative
7C	Mutagen	Positive	Positive	Medium risk	0	Positive
Erlotinib	Mutagen	Negative	Negative	Medium risk	0	Negative

*1= May be carcinogen; 0 = Non carcinogen.

ing the blood brain barrier (BBB), and to have an effect on the CNS activity (Table 3). The closer the carcinogenicity scores to one, the more likely a drug to be carcinogenic, while the closer the carcinogenicity scores to zero, the less the probably a drug to be carcinogenic. Table 4 indicated that, with the exception of compounds **5B**, **6B** and **7A**, the majority of the titled compounds are predicted to be safe (Prabhavathi et al. 2020).

Conclusions

Novel picolinic derivatives (**4–7**) were synthesized and confirmed by spectroscopic analysis, including ATR-FTIR, ¹HNMR, and CHNS. The MTT assay was used to assess their cytotoxic effects against two human cancer cell lines (A549 and MCF-7) as well as, non-tumorigenic MCF10A and WBC. Compound **5** exhibited anticancer activity against A549 lung cancer cells (IC₅₀ = 99.93 μM), but still had no effect on MCF-7 breast cancer cells or normal cells. Compound **5** exerted cytotoxicity in A549 lung cancer cells by inducing apoptosis, as made evident by fragmented nuclei after DAPI staining and agarose gel electrophoresis.

References

- Abbas A, Elias N, Fadhil A (2015) Synthesis, characterization and biological evaluation of new potentially active hydrazones of naproxen hydrazide. *Der Pharma Chemica* 7(10): 93–101.
- Abbas A, Mahmood A, Tahtamouni L, Al-Mazaydeh Z, Rammaha M, Alsoubani F, Al-bayati R (2021) New picolinic acid derivatives: Synthesis, docking study and anti-EGFR kinase inhibitory effect. *Materials Today: Proceedings*. <https://doi.org/10.1016/j.matpr.2021.05.354>
- Al-Saif F, Al-Humaidi J, Binjawhar D, Refat M (2020) Six new palladium(II) mixed ligand complexes of 2-, 3-, 4-monosubstituted derivative of pyridine ring with caffeine moiety: Synthesis, spectroscopic, morphological structures, thermal, antimicrobial and anticancer properties. *Journal of Molecular Structure* 1218: 128547. <https://doi.org/10.1016/j.molstruc.2020.128547>
- Amir M, Kumar H, Javed S (2007) Non-carboxylic analogues of naproxen: Design, synthesis, and pharmacological evaluation of some 1,3,4-oxadiazole/thiadiazole and 1,2,4-triazole derivatives. *Archiv Der Pharmazie* 340(11): 577–585. <https://doi.org/10.1002/ardp.200700065>
- Bai W, Ji J, Huang Q, Wei W (2020) Synthesis and evaluation of new thiourea derivatives as antitumor and antiangiogenic agents. *Tetrahedron Letters* 61(40): 152366. <https://doi.org/10.1016/j.tetlet.2020.152366>
- Bosco M, Rapisarda A, Massazza S, Melillo G, Young H, Varesio L (2000) The tryptophan catabolite picolinic acid selectively induces the chemokines macrophage inflammatory protein-1α and -1β in macrophages. *The Journal of Immunology* 164(6): 3283–3291. <https://doi.org/10.4049/jimmunol.164.6.3283>
- Chen Y (2015) Beware of docking! Trends in pharmacological sciences 36(2): 78–95. <https://doi.org/10.1016/j.tips.2014.12.001>
- Choi H, Yun W, Lee J, Jang S, Park S, Kim D, Seon K, Hyun J, Jeong K, Ku J, Nam T (2019) Synthesis and anti-endoplasmic reticulum stress activity of N-substituted-2-arylcarbonylhydrazinecarbothioamides. *Medicinal Chemistry Research* 28(12): 2142–2152. <https://doi.org/10.1007/s00044-019-02442-1>
- Furthermore, compound **5** activated caspases 3, 4, and 9. Moreover, when compared to vehicle-treated control cells, compound **5** treatment did not result in the release of cytochrome c from the mitochondria to the cytosol, however, it showed increased cytosolic Smac/DIABLO release. Finally, both compound **5** and thapsigargin increased eIF2 phosphorylation, proving activation of the ER stress pathway. A major problem in cancer treatment is chemoresistance, thus the search for new bioactive compounds that induce cancer cell killing in new and atypical mechanisms that avoid chemoresistance is of great interest. The current work demonstrated that the new derivative of picolinic acid, compound **5**, modulates ER stress to induce cancer cell death demonstrating its applicability in cancer treatment.

Acknowledgements

The authors sincerely acknowledge the support of Department of Pharmaceutical Chemistry, College of Pharmacy-University of Baghdad.

Conflicts of interest: The authors declare no conflicts of interest.

d'Azzo A, Tessitore A, Sano R (2006) Gangliosides as apoptotic signals in ER stress response. *Cell Death and Differentiation* 13(3): 404–414. <https://doi.org/10.1038/sj.cdd.4401834>

Da Cunha Santos G, Shepherd F, Tsao M (2011) EGFR mutations and lung cancer. *Annual Review of Pathology: Mechanisms of Disease* 6: 49–69. <https://doi.org/10.1146/annurev-pathol-011110-130206>

Dagur PK, McCoy Jr P (2015) Collection, storage, and preparation of human blood cells. *Current Protocols in Cytometry* 73(1): 1–16. <https://doi.org/10.1002/0471142956.cy0501s73>

Eissa I, El-Naggar A, El-Sattar N, Youssef A (2018) Design and discovery of novel quinoxaline derivatives as dual DNA intercalators and topoisomerase II inhibitors. *Anti-Cancer Agents in Medicinal Chemistry* 18(2): 195–209. <https://doi.org/10.2174/1871520617666170710182405>

El-Helby A, Sakr H, Eissa I, Al-Karmalawy A, El-Adl K (2019) Benzoxazole/benzothiazole-derived VEGFR-2 inhibitors: Design, synthesis, molecular docking, and anticancer evaluations. *Archiv Der Pharmazie* 352(12): 1–15. <https://doi.org/10.1002/ardp.201900178>

Fotakis G, Timbrell J (2006) In vitro cytotoxicity assays: Comparison of LDH, neutral red, MTT and protein assay in hepatoma cell lines following exposure to cadmium chloride. *Toxicology Letters* 160(2): 171–177. <https://doi.org/10.1016/j.toxlet.2005.07.001>

Fu J, Zhao L, Wang L, Zhu X (2015) Expression of markers of endoplasmic reticulum stress-induced apoptosis in the placenta of women with early and late onset severe pre-eclampsia. *Taiwanese Journal of Obstetrics and Gynecology* 54(1): 19–23. <https://doi.org/10.1016/j.tjog.2014.11.002>

Golemis E, Scheet P, Beck T, Scolnick E, Hunter D, Hawk E, Hopkins N (2018) Molecular mechanisms of the preventable causes of cancer in the United States. *Genes and Development* 32(13–14): 868–902. <https://doi.org/10.1101/gad.314849.118>

Harrison P, Vyse S, Huang P (2020) Rare epidermal growth factor receptor (EGFR) mutations in non-small cell lung cancer. *Seminars in*

- Cancer Biology 61(2019): 167–179. <https://doi.org/10.1016/j.sem-cancer.2019.09.015>
- Hmood K, Mahmood A (2020) Synthesis, docking study and *in vitro* anticancer evaluation of new derivatives of 2-(1-(2-fluoro-[1,1-biphenyl]-4-yl)ethyl)-6-(substituted phenyl) imidazole[2,1-B][1,3,4] thiaziazole derived from flurbiprofen. *Systematic Reviews in Pharmacy* 12(2): 184–201.
- Huang S, Zou X (2010) Advances and challenges in protein-ligand docking. *International Journal of Molecular Sciences* 11(8): 3016–3034. <https://doi.org/10.3390/ijms11083016>
- Jaszczyszyn A, Gąsiorowski K (2008) Limitations of the MTT assay in cell viability testing. *Advances in Clinical and Experimental Medicine* 17(5): 525–529.
- Khalil N, Kamal A, Emam S (2015) Design, synthesis, and antitumor activity of novel 5-pyridyl-1,3,4-oxadiazole derivatives against the breast cancer cell line MCF-7. *Biological and Pharmaceutical Bulletin* 38(5): 763–773. <https://doi.org/10.1248/bpb.b14-00867>
- King A, Wilson J (2020) Endoplasmic reticulum stress: An arising target for metal-based anticancer agents. *Chemical Society Reviews* 49(22): 8113–8136. <https://doi.org/10.1039/D0CS00259C>
- Masuda H, Zhang D, Bartholomeusz C, Doihara H, Hortobagyi G, Ueno N (2012) Role of epidermal growth factor receptor in breast cancer. *Breast cancer research and treatment* 136(2): 331–345. <https://doi.org/10.1007/s10549-012-2289-9>
- Mosmann T (1983) Rapid colorimetric assay for cellular growth and survival: application to proliferation and cytotoxicity assays. *Journal of Immunological Methods* 65(1983): 55–63. [https://doi.org/10.1016/0022-1759\(83\)90303-4](https://doi.org/10.1016/0022-1759(83)90303-4)
- Najeh Al-Saad H, Mahmood A, Al-Bayati R (2019) Design, synthesis, docking study and antiplatelet evaluation of new thiosemicarbazide derivatives derived from captopril. *Oriental Journal of Chemistry* 35(2): 829–838. <https://doi.org/10.13005/ojc/350246>
- Nawasreh M, Alzyoud E, Al-Mazaydeh Z, Rammaha M, Yasin S, Tahtamouni L (2020) Biological activity and apoptotic signaling pathway of C11-functionalized cephalostatin 1 analogues. *Steroids* 158(2): 108602. <https://doi.org/10.1016/j.steroids.2020.108602>
- Nisha C, Kumar A, Nair P, Gupta N, Silakari C, Tripathi T, Kumar A (2016) Molecular docking and *in silico* admet study reveals acylguanidine 7a as a potential inhibitor of β -secretase. *Advances in Bioinformatics* 2016: e9258578. <https://doi.org/10.1155/2016/9258578>
- Parrish A, Freel C (2013) Cellular mechanisms controlling caspase activation and function. *Cold Spring Harbor Perspectives in Biology* 5(6): a008672. <https://doi.org/10.1101/cshperspect.a008672> [PMID: 23732469]
- Patel C, Narechania M (2018) Targeting epidermal growth factor receptors inhibition in non-small-cell lung cancer: a computational approach. *Molecular Simulation* 44(17): 1478–1488. <https://doi.org/10.1080/08927022.2018.1515484>
- Prabhavathi H, Dasegowda K, Renukananda K, Karunakar P, Lingaraju K, Raja Naika H (2020) Molecular docking and dynamic simulation to identify potential phytochemical inhibitors for EGFR and HER2 as anti-breast cancer agents. *Journal of Biomolecular Structure and Dynamics*, 1–12. <https://doi.org/10.1080/07391102.2020.1861982>
- Rimawi M, Shetty P, Weiss H, Schiff R, Osborne C, Chamness G, Elledge R (2010) Epidermal growth factor receptor expression in breast cancer association with biologic phenotype and clinical outcomes. *Cancer: Interdisciplinary International Journal of the American Cancer Society* 116(5): 1234–1242. <https://doi.org/10.1002/cncr.24816>
- Sung H, Ferlay J, Siegel R, Laversanne M, Soerjomataram I, Jemal A, Bray F (2021) Global cancer statistics 2020: GLOBOCAN estimates of incidence and mortality worldwide for 36 cancers in 185 countries. *CA: A Cancer Journal for Clinicians* 71(3): 209–249. <https://doi.org/10.3322/caac.21660>
- Tahtamouni L, Nawasreh M, Al-Mazaydeh Z, Al-Khateeb R, Abdellatif R, Bawadi R, Bamberg J, Yasin S (2018) Cephalostatin 1 analogues activate apoptosis via the endoplasmic reticulum stress signaling pathway. *European Journal of Pharmacology* 818(2017): 400–409. <https://doi.org/10.1016/j.ejphar.2017.11.025>
- Tung C, Lu Y, Kao W, Liu J, Lai Y, Jiang S, Chen H, Shih T (2020) Discovery of a more potent anticancer agent than C4-benzazole 1,8-naphthalimide derivatives against murine melanoma. *Journal of the Chinese Chemical Society* 67(7): 1254–1262. <https://doi.org/10.1002/jccs.202000019>
- Van Geelen C, Pennarun B, Ek W, Le P, Spierings D, De Vries E, De Jong S (2010) Downregulation of active caspase 8 as a mechanism of acquired TRAIL resistance in mismatch repair-proficient colon carcinoma cell lines. *International Journal of Oncology* 37(4): 1031–1041. <https://doi.org/10.3892/ijo.00000755>
- Wang I, Lin-Shiau S, Lin J (1999) Induction of apoptosis by apigenin and related flavonoids through cytochrome c release and activation of caspase-9 and caspase-3 in leukaemia HL-60 cells. *European Journal of Cancer* 35(10): 1517–1525. [https://doi.org/10.1016/S0959-8049\(99\)00168-9](https://doi.org/10.1016/S0959-8049(99)00168-9)
- Wang Z (2017) ErbB receptors and cancer. In: Wang Z (Ed.) *ErbB Receptor Signaling. Methods in Molecular Biology*, vol 1652. Humana Press, New York, 3–35. https://doi.org/10.1007/978-1-4939-7219-7_1
- Westover D, Zugazagoitia J, Cho B, Lovly C, Paz-Ares L (2018) Mechanisms of acquired resistance to first- and second-generation EGFR tyrosine kinase inhibitors. *Annals of Oncology* 29(1): i10–i19. <https://doi.org/10.1093/annonc/mdx703>
- Wheeler D, Dunn E, Harari P (2010) Understanding resistance to EGFR inhibitors-impact on future treatment strategies. *Nature Reviews Clinical Oncology* 7(9): 493–507. <https://doi.org/10.1038/nrclinonc.2010.97>
- Xiong H, Cheng J, Zhang J, Zhang Q, Xiao Z, Zhang H, Tang Q, Zheng P (2020) Design, synthesis, and biological evaluation of pyridineamide derivatives containing a 1,2,3-triazole fragment as type II c-Met Inhibitors. *Molecules* 25(1): 1–16. <https://doi.org/10.3390/molecules25010010>
- Yaoxian W, Hui Y, Yunyan Z, Yanqin L, Xin G, Xiaoke W (2013) Emodin induces apoptosis of human cervical cancer hela cells via intrinsic mitochondrial and extrinsic death receptor pathway. *Cancer Cell International* 13(1): 1–8. <https://doi.org/10.1186/1475-2867-13-71>
- Yu X, Du J, Fan Y, Liu F, Cao L, Liang N, Xu D, Zhang J (2016) Activation of endoplasmic reticulum stress promotes autophagy and apoptosis and reverses chemoresistance of human small cell lung cancer cells by inhibiting the PI3K / AKT / mTOR signaling pathway. *Oncotarget* 7(47): 76827. <https://doi.org/10.18632/oncotarget.12718>
- Zeidan M, Mostafa A, Gomaa R, Abou-zeid L, El-Mesery M, El-Sayed M, Selim K (2019) Design, synthesis and docking study of novel picolinamide derivatives as anticancer agents and VEGFR-2 inhibitors. *European Journal of Medicinal Chemistry* 168: 315–329 <https://doi.org/10.1016/j.ejmech.2019.02.050>
- Zhang Q, Chen M, Cao L, Ren Y, Guo X, Wu X, Xu K (2020) Phenethyl isothiocyanate synergistically induces apoptosis with Gefitinib in non-small cell lung cancer cells via endoplasmic reticulum stress-mediated degradation of Mcl-1. *Molecular Carcinogenesis* 59(6): 590–603. <https://doi.org/10.1002/mc.23184>
- Zheng S, Liu T, Liu Q, Yang L, Zhang Q, Han X, Shen T, Zhang X, Lu X (2020) Widely targeted metabolomic analyses unveil the metabolic variations after stable knock-down of NME4 in esophageal squamous cell carcinoma cells. *Molecular and Cellular Biochemistry* 471(1–2): 81–89. <https://doi.org/10.1007/s11010-020-03768-w>